The Pennsylvania State University

The Graduate School

POLARITY DISPARITY GOVERNS HIERARCHICAL ARRANGEMENTS IN MULTIPHASE CONDENSATES

A Thesis in

Chemistry

by

Yuqi Tang

Submitted in Partial Fulfillment
of the Requirements
for the Degree of

Master of Science

December 2021

The thesis of Yuqi Tang was reviewed and approved by the following:

Xin Zhang
Paul & Mildred Berg Early Career Professor
Associate Professor of Chemistry
Associate Professor of Biochemistry and Molecular Biology
Thesis Advisor
Chair of Committee

Tae-Hee Lee
Professor of Chemistry

Ruobo Zhou
Assistant Professor of Chemistry
Assistant Professor of Biomedical Engineering

Philip C. Bevilacqua
Distinguished Professor of Chemistry
Distinguished Professor of Biochemistry and Molecular Biology
Head of the Chemistry Department

ABSTRACT

Phase separation is a process through which a homogenous mixture of macromolecules spontaneously segregates into two distinct phases, usually a condensed phase surrounded by a dilute phase. Eukaryotic cells apply this strategy in forming membraneless organelles to dynamically regulate complex biochemical reactions. Aberrant phase transitions of these membraneless organelles are associated with disease phenotypes. Despite this long-established appreciation, how phase separation occurs to form biological condensates and how multiple sub-compartments are regulated within condensed phase remain enigmatic. Many studies have proposed sophisticated theories regarding the biophysical and molecular grammar that might regulate phase behaviors of condensates both *in vitro* and in cells. However, the physical and chemical principles that regulate multi-component protein condensates still remain elusive. Recent findings in our lab suggested that polarities of subcompartments play crucial roles in regulating the formation and organization of multilayered droplets through simplified polypeptide model—elastin-like polypeptides (ELPs). In particular, ELPs with low polarity difference are prone to form single phase protein condensates, whereas ELPs with high polarity difference are envisioned to form multiphase droplets, resembling "core-shell" structures, with more polar ELP is partitioned in the shell layer. The research covered in this thesis, introduced endogenous tau protein to the existing ELP system, and the structures of droplets formed between tau and V_2I_7E40 were successfully modified through the addition of polyU. The interaction between tau protein and polyU reduced the polarity of tau protein, causing previously miscible V_2I_7E40-tau droplets to segregate into layered core-shell structures. Therefore, this work provided strong evidence supporting the notion that polarity plays an important role to determine substructure of multi-component condensates. This knowledge may serve as a general principle that could be applied in explaining the organization of macromolecules within biological condensates.

TABLE OF CONTENTS

LIST OF FIGURES

ACKNOWLEDGEMENTS

I would like to express my deepest appreciation to my thesis advisor **Prof. Xin Zhang**, for his solid training on my scientific skills and critical thinking. He was not only my advisor but also truly a scientific and life mentor. I would like to specially thank him for his kindly help and unconditional support during the pandemic year even though we haven't met. I truly appreciated his acceptance of me joining his lab and his generous support on my exploration of scientific projects. His passion for science has greatly encouraged me a lot in my pursue of academic studies.

I would also like to extend my sincere thanks to the rest of the members in my committee, **Prof. Tae-Hee Lee**, and **Prof. Ruobo Zhou**. They created a cooperative atmosphere and provided useful feedback on my study. Without their help and guidance, I would have never been able to complete my thesis.

Special thanks to my mentor **Songtao Ye**, who patiently taught me all the experimental skills and underlying theories. I learned a lot from his vast biochemistry and physical chemistry knowledge, and benefited from his critical scientific insight as well as his patience in trouble-shooting problems. He is truly a great mentor and an excellent friend. I'd also like to extend my gratitude to **Henry Hsiung**, **Leman Simpson**, and other lab members that I have enjoyed working with.

I would like to extend my sincere thanks to my beloved **family**. I would have never gone this far with their unconditional love and support.

Last but not least, I would like to thank Pew Research Center for its resource to support this thesis. Any opinions, findings, and conclusions or recommendations expressed in this thesis are those of the author myself and do not necessarily reflect the views of the Pew Research Center.

Chapter 1

INTRODUCTION

Membraneless Organelles

Eukaryotic cells require precise spatial and temporal regulation over their complex biochemical reactions to function properly, such compartmentalization is often accomplished in specific organelles. These compartments, such as mitochondrion or lysosomes, are commonly segregated by lipid membranes, in which the maximum efficiency of specialized biochemical reactions is achieved. However, many cellular compartments do not have defined membranes, yet they are envisioned to have a wide range of cellular functions ranging from RNA metabolism to gene regulation. Those are called membraneless organelles, or biological condensates. Advances in cell biology and microscopy have divulged a handful of biological condensates. Since the observation of nucleolus within the nucleus of neuronal cells in the 1830s[1], membraneless organelles have been discovered within the nucleus, cytoplasm and on membranes of essentially all eukaryotic cells. Examples include Cajal bodies, promyelocytic leukemia (PML) bodies, stress granules, and germ granules. The nucleolus is the most prominent membraneless organelle in the nucleus and responsible for ribosome biogenesis[2]. Cajal bodies are mainly associated with the production of small nuclear ribonucleoproteins (snRNPs) that catalyze RNA splicing[3]. Studies on germline P-granules in *C. elegans* (Figure **1-1**) provided the experimental evidence that suggested the liquid-like properties of these condensates including: (1) many of them exhibit spherical morphologies; (2) they can display fusion events as well as wetting behaviors; (3) they are able to exchange cellular components with their surrounding environment within seconds.

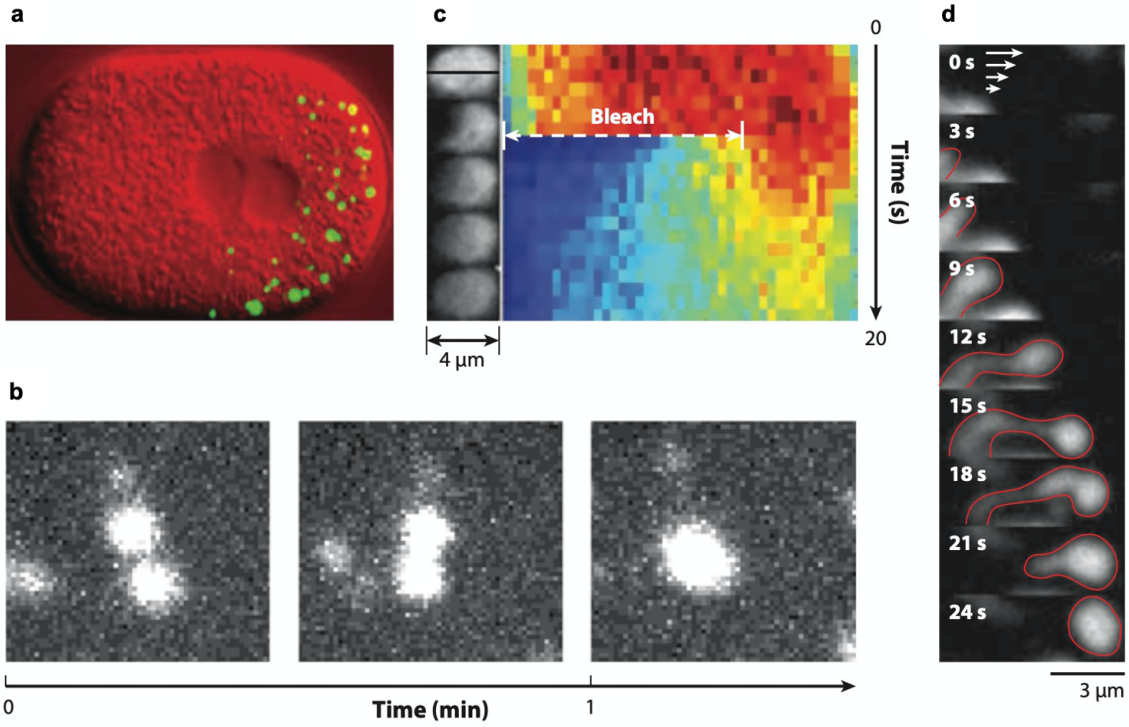

Figure **1-1**: P-granules exhibit liquid-like properties. (a) GFP-tagged P-granules (green) in the cytoplasm of a one-cell stage C.elegans embryo. (b) Two P-granules (white) fuse within about one minute. (c) Fluorescence distribution before and after photobleaching of a large GFP-tagged P granule (left). Kymograph of linear intensity profiles along the anterior-posterior axes (right). Red color indicates high intensity and blue corresponds to background intensity. Fluorescence recovery occurs in about 5 s. Figure adapted from reference 4.

Liquid-liquid Phase Separation

The unifying principle that governs the self-assembly of these liquid-like condensates is a physical process called liquid-liquid phase separation (LLPS). With a mean-field estimate for homopolymer solutions, the Flory-Huggins solution theory applied lattice model to calculate the free energy of mixing through the combination of entropy and energy of mixing. The simple dimensionless form of Flory-Huggins equation could be written as:

$$\frac{\Delta F_m}{k_B T} = \frac{\emptyset}{N}\ln(\emptyset) + (1-\emptyset)\ln(1-\emptyset) + \chi\emptyset(1-\emptyset) \qquad 1$$

In Equation 1, ΔF_m refers to the change of free energy; *N* stands for the number of sites occupied by individual polymer segments; $\emptyset$ is the volume fraction of polymers; and χ is the Flory interaction parameter. In the simple homopolymer model, there present three types of interactions: polymer-polymer, solvent-solvent, and polymer-solvent. The tendency for this system to undergo phase separation into polymer-rich condensed phase and polymer-depleted dilute phase is determined by χ, which quantifies the competition among these interactions and is defined as:

$$\chi = \frac{z\left(2u_{\mathrm{ps}} - u_{\mathrm{pp}} - u_{\mathrm{ss}}\right)}{2k_{\mathrm{B}}T} \qquad 2$$

The terms u_{pp}, u_{ss}, u_{ps} refer to mean-field energies for interactions between polymers and solvents or polymer-solvent, respectively. z is a coordination number that represents the average number of nearest-neighbor interactions that each monomeric unit within the polymer can make. In good solvent, $\chi < 0$, which means that polymer-solvent interactions are dominant. Therefore, a homogenous, one-phase solution is preferred. Conversely, $\chi > 0$ when in poor solvent, reflecting that polymer-solvent interactions are minor, leading to the formation of two coexisting phases.[5]

The Flory-Huggins theory has laid solid foundation in explaining the phase separation of simple polymers and agreed well with many experimental results. However, for macromolecules within cellular environment, the situation is far more complex. Unlike simple polymers, many of these endogenous proteins have well-defined three-dimensional structures, which could alter in accordance with cellular process. Additionally, there always presents multivalent interactions among these macromolecules within specific domains. All these factors, together with surrounding environment, make the prediction of phase separation by simply Flory-Huggins theory impossible.

There are several potential modes of molecular interactions that are known to promote intracellular phase transitions[6]. They include electrostatic interactions between two charged residues, cation-π interactions between a positively charged residue and an aromatic residue, π-π stacking between two aromatic residues, dipole-dipole interactions between two polar residues.

Collectively, these molecular interactions are called multivalent interactions (Figure **1-2a**). In cellular environment, these interactions are normally mediated by macromolecules such as protein, RNA, and DNA. A key principle in the assembly of such biological condensates is multivalent interactions between protein-protein as well as protein-RNA. This multivalency is achieved through modular interaction domains within proteins. For example, RNA-binding proteins (RBPs) are usually composed of a prion-like domain (PrLD) and several RNA-binding domains (RBDs). Prion-like domain is one specific type of intrinsically disordered region and is often reported to drive phase separation of many RBPs by itself, whereas RBDs could only function to promote phase separation through their interactions with RNAs or other domains. Besides, recent studies suggest that oligomerization domains can also contribute to phase separation of some proteins such as TDP-43[7].

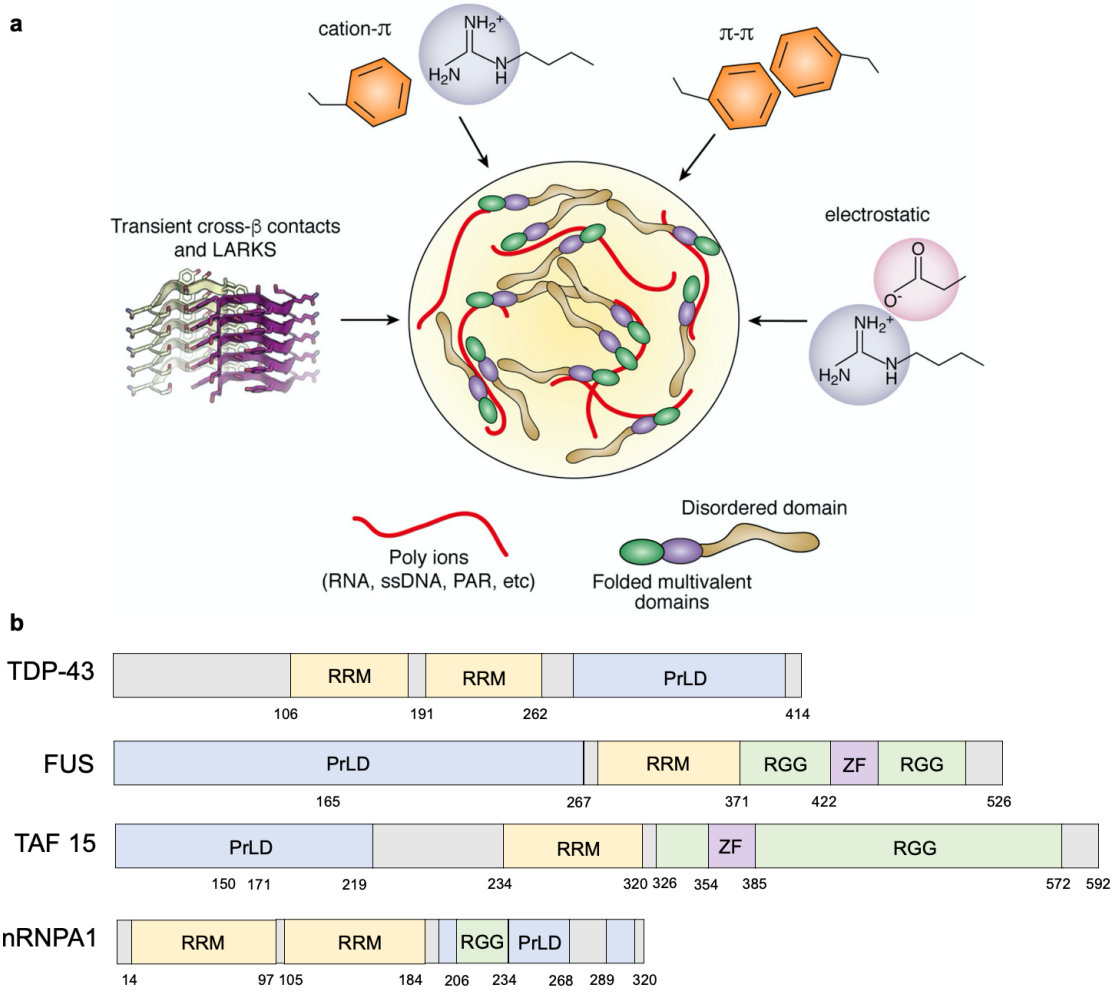

Figure **1-2**: (a) Modes of interactions that participate in LLPS. LARKS: low- complexity, aromatic-rich, kinked segments. (b) Representation of PrLD and RBDs in several RBPs that could undergo phase separation. RRM: RNA recognition motif. RGG: arginine-glycine-glycine. ZF: zinc finger. Figure (b) modified from reference 8.

Intrinsically Disordered Regions and Associated Proteins

A large portion of proteins that phase separate into droplets contains intrinsically disordered regions (IDRs), which are unable to fold into well-defined three-dimensional structures under physiological conditions. Proteins with entirely disordered sequences are called intrinsically disordered proteins (IDPs). However, the majority (~58%) of cellular proteins are made up of both IDRs as well as structured regions. These IDRs are compositionally biased with a depletion of

bulky hydrophobic residues that drive higher-order folding, but typically enriched in polar residues such as serine (S), glutamine (Q), and asparagine (N); charged residues such as lysine (K), arginine (R), and aspartic acid (D); aromatic residues such as tyrosine (Y) and phenylalanine (F)[9]. Such feature has allowed many IDR-containing proteins to phase separate both *in vitro* and in cells. For example, Ddx4, an RNA-binding protein that has extended IDRs in both N and C termini. It is reported that phase separation of Ddx4 is predominantly driven by electrostatic interactions between oppositely-charged clusters of length 8-10 residues and cation-π interactions between FG and RG pairs[10].

Structures and Functions of Tau Protein

The tubulin-associated unit (tau) is also one of the IDR-containing proteins[11]. In healthy conditions within cells, tau is predominantly expressed in the neurons and critical in regulating the assembly and stability of microtubules (MTs). However, under adverse conditions, tau is no long bound to neuron but solubilized in cellular environment. Under these conditions, tau forms insoluble, high molecular weight filaments, which are associated with over 20 neurodegenerative diseases[12-15]. Examples include Alzheimer's disease, argyrophilic grain disease, and Pick's disease. Even though much work has been done regarding the cause of these pathological diseases, we still do not fully understand the principle that regulates the transition from soluble tau protein to disease related fibrils.

Through extensive isolation and characterization, people have identified six isoforms of tau ranging from 352 to 441 amino acids in length expressed in adult human brain[16]. Generally, there are around 150 residues in the N-terminal and 70 residues in the C-terminal of tau and the microtubule-binding region located in between. Both N-terminal and C-terminal are largely disordered whereas the microtubule-binding region could adopt a helical structure when bound to

microtubules. There is N-terminal extension of 29 or 58 amino acid residues with one or two inserts (tau0N, tau1N, and tau2N), and a lack of one repeat domain out of four repeats in the microtubule-binding region (total four repeats comprise residues 244-368) (Figure **1-3**). Each repeat has similar structure, displaying a characteristic Pro-Gly-Gly-Gly motif, which might contribute to the rapidly growing protofilaments[16,17].

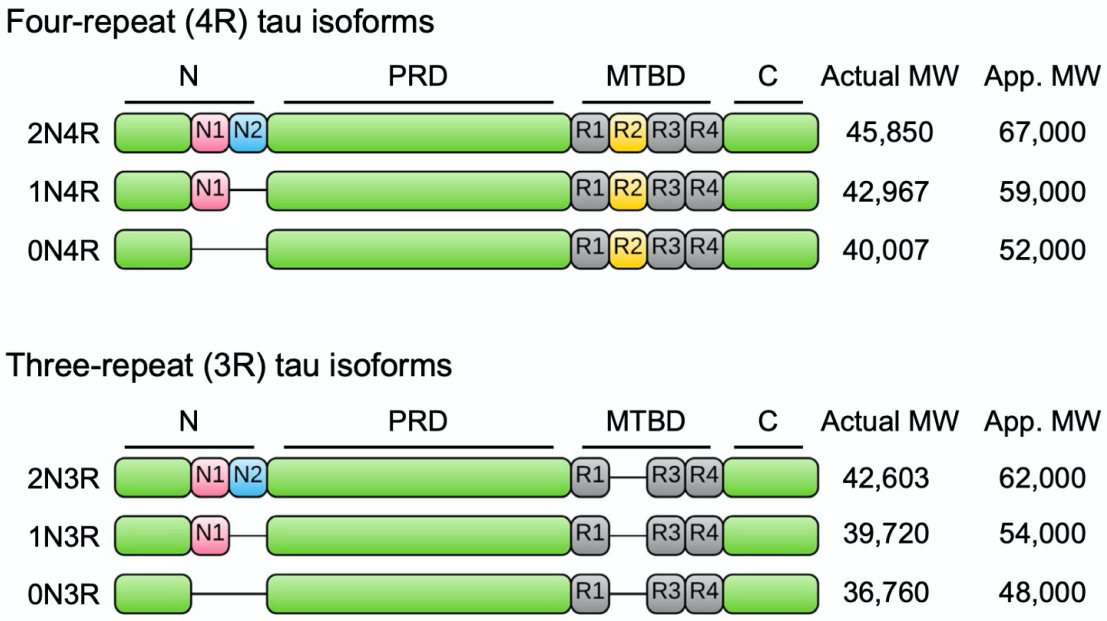

Figure **1-3**: Structure representatives of six isoforms of tau. Full-length 2N4R is the longest isoform of tau that has both N-terminal extension as well as the presence of the second repeat domain on the microtubule-binding domain (MTBD). N: N-terminal of tau. C: C-terminal of tau. PRD: prion-like domain. App. MW: apparent molecular weight, kDa. Figure adapted from reference 18.

Numerous studies showed that post-translational modifications are regulators of many neurodegenerative proteinopathies, there is also no exception for tauopathies. Truncation is one of the post-translational modifications in tau that might impede the functional properties and trigger pathological fibrils. In Alzheimer's disease, truncations usually happen at either N-terminal or C-terminal site. Remarkably, studies suggests that N-terminal truncation may hinder its stabilization of microtubule, as well as influence the polymerization and localization of tau itself[19]. Therefore,

extensive studies based on the N-terminal truncated tau could possibly help us gain more insights into the role of tau in cellular functions, and progression of tauopathies.

Tau187-RNA Complex Coacervation

Tau187 is one truncated version of the longest tau isoform that contains four repeat domains (R1-R4) and the entire C-terminal regions. Despite the fact that tau187 lacks RNA-recognition motif, it can still phase separate into droplets upon complexation with RNA[20,21] (Figure **1-4**). Typically, complex coacervation refers to a phase separation process caused by interactions between two oppositely-charged macromolecules. This process is normally modulated by electrostatic interaction; however, it can also be facilitated by cation-π interactions as well as hydrophobic interactions. Based on the type of macromolecules that participate in phase separation, there are three types of complex coacervate systems: polyelectolyte-polyelectrolyte systems, polyelectrolyte-charged surfactant systems, and zwitterionic systems[22]. Tau187-RNA coacervate typically belongs to the first type, even though both tau187 and RNA are biomolecules that are distinct from synthetic polymers.

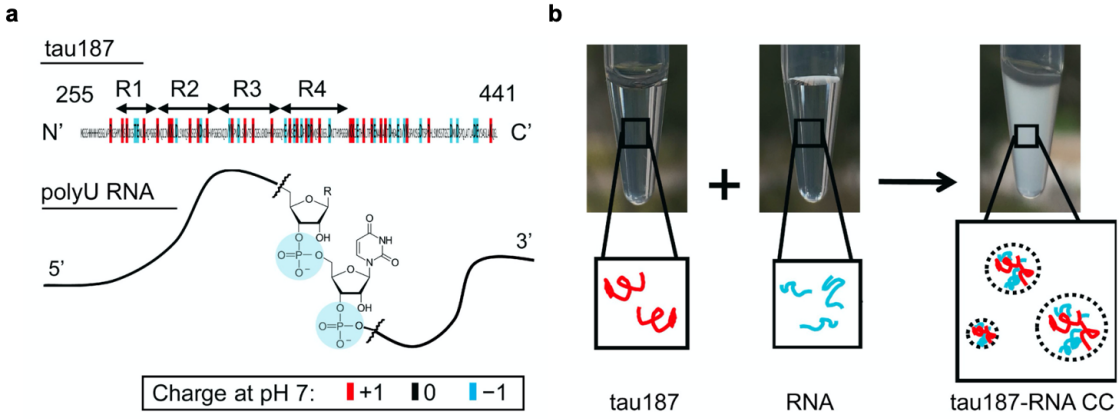

Figure **1-4**: Tau187 and RNA form complex coacervates. (a) Schematic representation of tau187 and polyU RNA. Tau187 contains four repeat domains as well as C-terminal domain with a net

positive charge at neutral pH. (b) Mix tau187 and polyU at certain conditions results in a cloudy solution. Figure adapted from reference 21.

Interestingly, unlike many RBPs that require specific RNA to phase separate, tau187 can form coacervates with different RNA types such as tRNA, polyU, and polyA. This general trend suggests that interactions between tau187 and RNA are nonspecific. Remarkably, the droplet formation is maximum when the charge ratio between positively-charged tau187 and negatively-charged RNA reaches around 1:1. The formation of tau187-RNA coacervates is reversible and can be tuned by temperature, salt concentration, as well as tau187:RNA ratio (Figure **1-5**). The majority of tau187 are shown to assume their dynamical conformations when coacervate with RNA even for a long time (>15 hours). However, concentrated tau187 within droplets could facilitate aggregate formation once unfavorable factors are introduced[20]. This observation suggests that phase separation of tau might serve as a median process that promotes the formation of tau fibrils towards tauopathies.

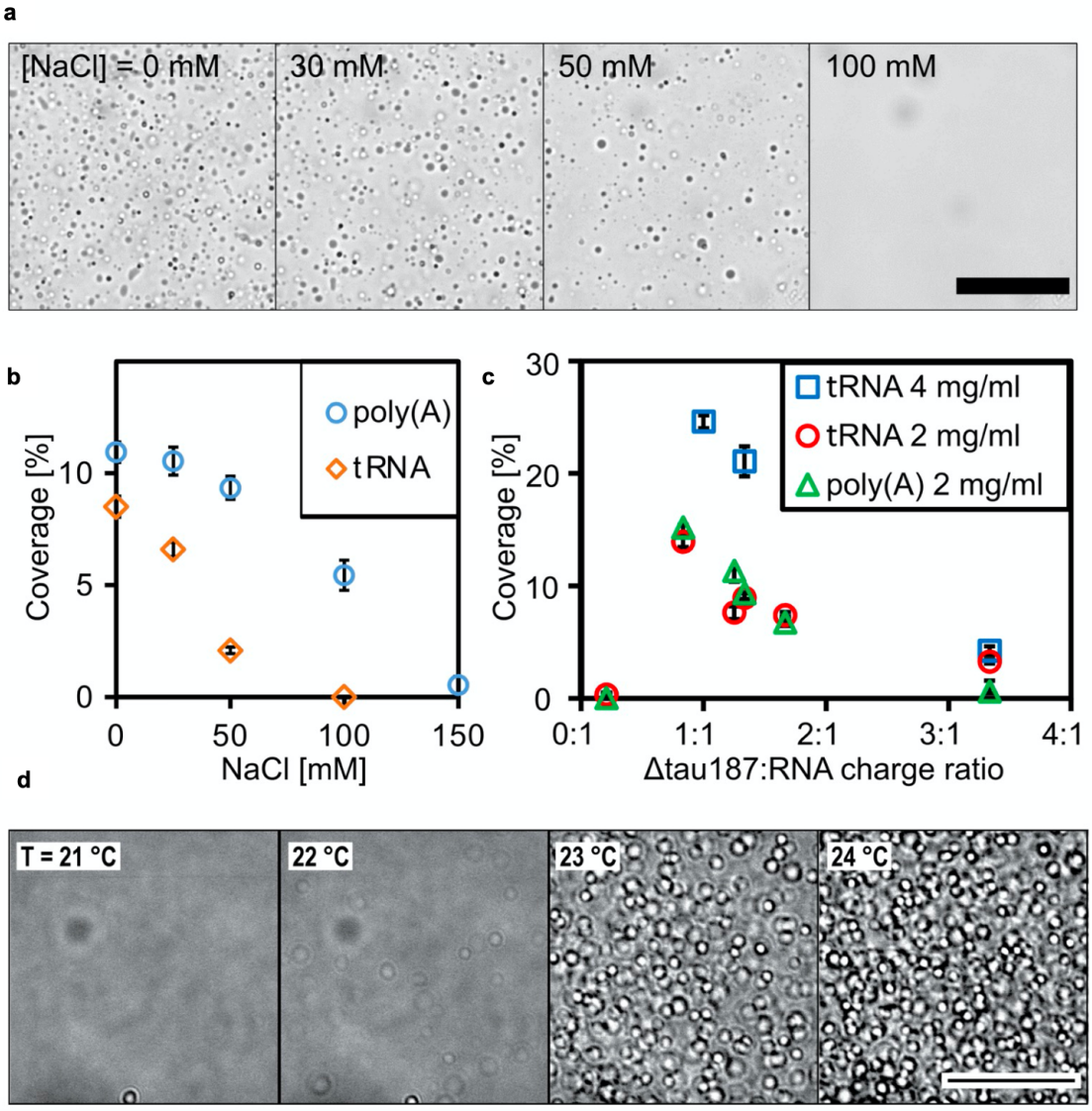

Figure **1-5**: Tau187-RNA complex coacervation can be tuned by several factors. (a) and (b) Increasing in salt concentration decreased the amount of tau187-RNA droplets. However, droplets formed with polyA shows higher tolerance towards the increase. Tau187:RNA were mixed at a mass ratio of 7:1 (charge ratio of 1.2:1) and a total mass concentration of 2 mg/ml. (c) Droplet formation changes with varying tau187:RNA ratio. Specifically, the formation reaches to the maximum when the charge ratio between tau187 and RNA is around 1.2-1.3, regardless of RNA type. (d) Slightly difference in temperature results in distinct droplet formation. Figure adapted from reference 20.

Elastin-like Polypeptide

Elastin-like polypeptides (ELPs) are artificial polypeptides that contain repeats of the pentapeptide sequence Val-Pro-Gly-X-Gly, where X (also called guest residue) could be any naturally occurring amino acid residue except proline and n is the number of repeat units. Proline residues in the repeat sequence promote chain rigidity whereas glycine motifs contribute to flexibility.[23] The combined PG dipeptide acts as a spacer between helical turns in the formation of β-spiral structure. Therefore, if the guest residue X is proline, the formation of helical structure of ELP would be disrupted.[24] The repeat sequence is derived from the hydrophobic domain of tropoelastin, which is an important component in providing elasticity to tissues such as arteries, lungs, and skin through coacervation (Figure **1-6**)[25].

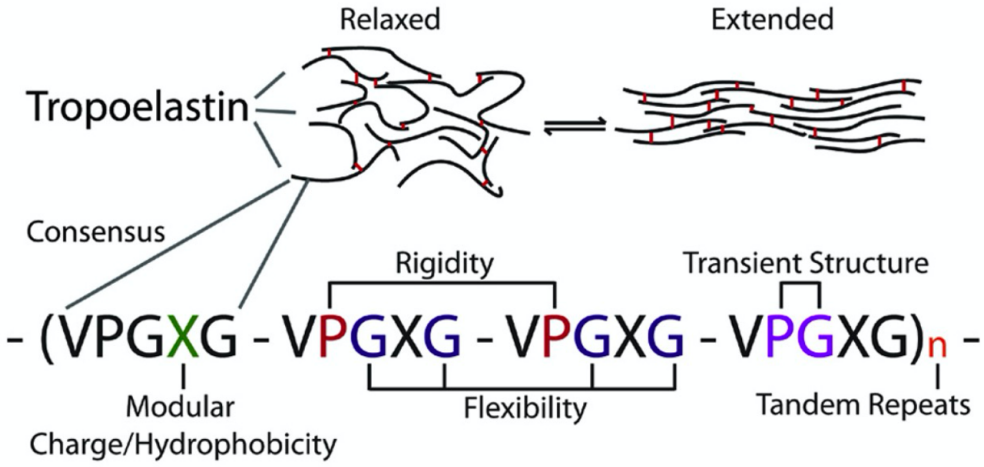

Figure **1-6**: ELP derived from the hydrophobic domain of tropoelastin. Figure adapted from reference 26.

Lower Critical Solution Temperature

Just like tropoelastin, these polypeptides can undergo reversible, thermally triggered lower critical solution temperature (LCST) type phase transition, in which the elevation of temperature could result in the phase separation of ELP and the formation of protein-rich droplets. This process could be explained by the Gibbs energy of mixing ($\Delta G_m = \Delta H_m - T\Delta S_m$). ELPs are overall hydrophobic macromolecules compared to water molecules. When the former are placed into an aqueous environment, water molecules surrounding them are packed into "cages", which leads to an entropy loss ($\Delta S_m < 0$) due to the restriction of the movement, or enhanced ordering of water molecules. However, the presence of hydrogen bonds between ELP and water molecules contributes to ΔH_m negatively. In this situation, temperature plays a crucial role in determining the sign of ΔG_m, which changes at a critical phase transition temperature ($T_t = \Delta H_m / \Delta S_m$) that corresponds to the LCST in our ELP system. Beyond LCST, the entropic term $T\Delta S_m$ predominates, yielding a positive value in the change of Gibbs energy, hence ELP phase separate into droplets.[27-29] In short, it is suggested that the LCST phase transition of ELP is an entropy-driven event.

The LCST of ELP can be affected by several factors such as guest residue, chain length, polypeptide concentration as well as ionic strength. ELPs are genetically encodable and easily synthesized by heterologous overexpression from a synthetic gene with precise control over their composition and chain length. These unique properties make ELPs attractive in a wide range of applications, such as drug delivery, recombinant protein purification, tissue engineering[30]. As the highly repetitive pentapeptide motifs suggest that ELPs are completely disordered polypeptides with extremely simple amino acid residues, and given the fact that there is more sophisticated understanding of their phase behavior, ELPs can also serve as models in studying the fundamental mechanism governing the phase separations of IDPs in biological process.

Multiphase Organization

In many cases, cellular compartmentalization of multicomponent requires the coexistence of multiple domains or layers, in which biomolecular processes take place in physically separated regions. However, our understanding of the underlying principles is still elusive, and the rules for the coexistence of condensed phase are extremely limited. Nevertheless, scientists have proposed several hypotheses guiding the hierarchical arrangement in multiphase condensates.

A study concerning *X. laevis* nucleoli by Feric[31] demonstrated that the organization of the immiscible multiphases is regulated by their surface tensions. Nucleoli was previously reported to have three distinct layers: granular components (GCs), dense fibrillar components (DFCs) and fibrillar centers (FCs)[32]. Remarkably, through extensive purification they found that both FIB1 (enriched in DFCs) and NPM1 (enriched in GCs) can undergo LLPS *in vitro* individually in the presence of rRNA. And they coexist as multiphase droplets when mixed together *in vitro*, in which the typical "core-shell" structure is also observed *in vivo* studies. To gain molecular insights into the driving force underlying the formation of such multiphase droplets, they conducted substantial domain studies and found that the RNA-binding domains are crucial in multiphase formation. More importantly, noticing that different layers of droplets have distinct biophysical properties through biophysical characterization and wetting behavior, and in combination with polymer theories in solutions, they revealed such organization is driven by differences in surface tension.

Despite the fundamental guidance laid here, our understanding of the biomolecular determinants of condensate surface tensions, and the potential role of any surfactant-like biomolecules in modulating these interfacial properties, is still lacking.

Simon[33] applied ELPs as model to study the underlying rules govern the phase behavior of multicomponent IDP-rich droplets *in vitro*. Despite there are substantial difference in the sequences of ELPs and intracellular IDPs, they share key features such as highly repetitive, low complexity,

and disorder in solution. After confirming that layered core-shell coacervates could form in the solutions of combining ELPs, they further investigated underlying mechanism governing the formation of multilayer structures based on sequences of ELPs. Through extensive modification and Flory–Huggins (FH) phase diagram predictions, they found that sequence composition, molecular weight and concentration all influence the multilayer structures. Specifically, they proposed that ELPs with similar amino acid compositions are prone to form mixable condensates whereas for those with distinct compositions tend to form multilayered condensates. Exception for the latter scenario could be the decrease in molecular weight or chain length. Their understandings of sequence rules governing the formation of multilayer structures are of great importance in studying phase behaviors of cellular IDPs and provide us with inspirations on designing biomaterials that could be applied in medical field.

However, there are still many macromolecules that are much unlike ELPs present in biological condensates. They could contain a significant amount of charged residues, such as RNA-binding proteins and RNA, and the formation of condensates are mainly due to electrostatic interactions among them. In this circumstance, is there any possibility that multilayered phase still occurs? If so, what's the underlying rule that control these hierarchical multiphase organizations?

Lu[34] answered these questions using complex coacervates as model systems. Complex coacervates are liquid droplets formed mainly by electrostatic interactions between oppositely charged macromolecules. Firstly, by mixing two kinds of positively charged polymers with ssDNA together they observed a multiphase formation with two droplets separated by a sharp and smooth interface. Using fluorescent microscopy imaging they found that the only polyanion among them all is present in both phase, which suggests attraction interactions both occur between ssDNA and other two polymers in the core and the shell. However, there is higher distribution of ssDNA in the core suggested by fluorescence intensity. And similar results could also be seen in other charged multicomponent mixtures. Through extensive phase separation experiments using various

molecules, they observed that chemical characteristics have nothing to do with the regulation of multiphase droplets. However, through comprehensive analysis regarding the physical theory of interfacial energy, they revealed that the formation of multiphase droplets requires the interfacial tension between two coacervates lower than the interfacial tension of one of the coacervates with surrounding dilute phase. Moreover, by combining Flory−Huggins theory with experimental evidence, they further illustrated the hierarchical organization of multiphase droplets using density differences between complex coacervates. In the multiphase droplets formed, core coacervates usually have higher density and low water content. In conclusion, through systematic analysis and substantial experiments, they present us with a general mechanism that regulate the formation and hierarchical organization of multiphase droplets *in vivo*, which hopefully, could be applied in biological systems as well as modular design for multi-functional self-organized compartments.

Environmental Sensitive Fluorophores

The physicochemical properties (such as pH, temperature, viscosity, and polarity) within cellular environment play important roles in reporting cellular status and respective behaviors. Aberrant changes in these properties are sometimes connected with cellular dysfunctions. For example, protein aggregation is the hallmark of many neurodegenerative disease. Normally these proteins are well-folded in cellular environment and function properly. However, upon a disturbance in cellular environment or mutations, these proteins transition to soluble oligomers, and ultimately insoluble aggregates. During this process, the hydrophobic core is disrupted and exposed to the hydrophilic environment. Therefore, the polarity of the local environment is changed.

To have a detailed dissection of biological processes, various environmental sensitive fluorophores have been developed to monitor the physicochemical properties of local environment. These fluorophores can serve as the most sensitive tool in reporting the polarity, viscosity, as well

as molecular of their environment. Unlike traditional "always-on" fluorophores that require a washing process to get rid of high background fluorescence of unbound fluorophores, these environmental sensitive fluorophores are largely nonfluorescent due to both inter- and intramolecular nonradiative decay[35,36]. However, alterations in certain physicochemical property may lead to a great enhancement in the fluorescent intensity and/or an observable shift in the maximal emission wavelength.

The classical polarity sensitive fluorophores are solvatochromic dyes exhibiting push-pull structures. This typical structure enables the charge transfer from the donor group to the acceptor and thus form highly dipolar excited state after light absorption (10^{-15} seconds). The excited state is highly unstable, which could immediately interact with the dipoles of surrounding solvent through relaxation (10^{-10} seconds). The solvent-mediated external conversion hence reduces the energy gap between ground state (S_0) and excited state (S_1) and introduces a red shift in the emission spectra. As such, the emission shifts to longer wavelength in more polar solvents. Owing to their sensitivity to environmental polarity, various push-pull solvatochromic dyes and their derivatives have been applied to monitor intrinsic biophysical properties of biological systems. Examples include Nile Red[37], Dansyl[38], FR0[39], etc. Many studies have modified their polarity sensitive fluorophores based on the solvatochromic fluorophore 4-sulfamonyl-7-aminobenzoxadiazole (SBD) and applied them in different biological systems. Zhuang et al[40] conjugated SBD to protein-specific ligand to detect native enzymes. SBD is nonfluorescent when in polar environment due to solvent-mediated external conversion, but shows strong fluorescence and blue-shifted emission in hydrophobic environment. Given the fact that most ligand-binding sites within proteins have a hydrophobic environment, the fluorescence turn-on of SBD can be achieved upon ligand binds to its target protein. Our lab recently developed a proteome stress sensor based on SBD and applied them in quantifying proteome stress[35]. The sensor is composed of a destabilized protein tag as well as an SBD fluorophore. Under varying stress conditions, the protein tag can adopt a misfolded state

or aggregated state, in which the polarity changes accordingly. Then the polarity change can be sensed by conjugated SBD through a measurable intensity enhancement.

Fluorescence Lifetime Imaging Microscopy

Fluorescence microscopy is a powerful tool used to deliver spatial and functional information about cellular component on the molecular scale. Traditional fluorescence microscopy is usually based on the analysis of fluorescence intensity or fluorescence spectrum. However, except for these two parameters, fluorescence lifetime (τ) has also gained much attention in recent years. Fluorescence lifetime is defined as the average time that a population of fluorophores remains in their excited state before returning to the ground state[41]. Conventionally, fluorescence lifetime is considered as a kinetic parameter that inversely proportional to the sum of rate constants of a radiative process k_r and cumulative nonradiative processes k_{nr} (eq 3).

$$\tau = \frac{1}{(k_r + k_{nr})} \tag{3}$$

It could also be stated that the fluorescence lifetime is the time required for fluorescence intensity of fluorophores to reach to 1/*e*, or 36.8%. Unlike fluorescence intensity, fluorescence lifetime does not depend on the actual concentration of the fluorophore, light-path length, nor the duration of light exposure, which are hard to control or even unknown within cells. Instead, it depends on intrinsic fluorophore structure and could be affected by external factors such as temperature, pH, ion and oxygen concentrations, polarity, as well as molecular interaction by energy transfer when two proteins approach each other. Therefore, fluorescence lifetime is highly variable and can report on how long the fluorophore has to react with the environment.

Based on all those merits, fluorescence lifetime imaging microscopy (FLIM) emerged and has gained popularity in studying biological systems. Time-correlated single-photon counting

(TCSPC) is one of the well-established and widely used FLIM techniques. It detects single photons and measures their time of arrivals upon excitation by pulsed lasers. With multiple cycles of data collected at each pixel, an exponential fluorescence decay curve can be fitted, from which the mean lifetime could be determined. Then the fitting result from each pixel could be color mapped into an image with corresponding histogram plotted in parallel.

Chapter 2

RESULTS AND DISCUSSION

Introduction

The concept of surface tension and interfacial tension in regulating the multiphase organization may be compelling, however, it is difficult to measure this parameter, especially in live cells with highly dynamicity. The prediction on the phase behavior of multicomponent system solely based on their sequences is impossible. Therefore, I tend to interpretate the underlying mechanism of multiphase organization through a more general and visualizable way by introducing environmental sensitive fluorophores.

Another graduate student Songtao Ye in our lab discovered that three structures of droplets formed *in vitro* when mixing two ELPs together and promote phase separation above the critical temperature for both constructs. These structures are including fully miscible one-layer droplets, and partially miscible bilayer droplets, immiscible bilayer droplets with core-shell character. Through labeling ELPs with home-made polarity sensitive fluorophore SBD and viscosity sensitive fluorophore BODIPY (Figure **2-1**b), FLIM experiments were conducted, revealing that individual ELP droplets possess different polarities as well as viscosities. When comparing these data with their respective phase behavior, it is interesting to note that the phase behavior of two ELPs is in correlation to the polarity instead of viscosity. Furthermore, phase separation experiments were carried out for two-ELP systems and polarities of both ELPs within droplets were quantified using FLIM experiments. We found that the conformation of ELP condensates is determined by the polarity difference ($\Delta\boldsymbol{\varepsilon}$) of their component ELPs. Fully miscible one-layer droplets are formed when $\Delta\boldsymbol{\varepsilon}$ is small. However, as $\Delta\boldsymbol{\varepsilon}$ increases, partially miscible bilayer droplets may occur, and

when Δ**ε** is large enough, they are found to form immiscible bilayer droplets with core-shell character. Whereas, in bilayer droplets, the component that shows comparatively higher polarity is always located in the shell, whereas the one with lower polarity is localized in the core (Figure **2-1**c).

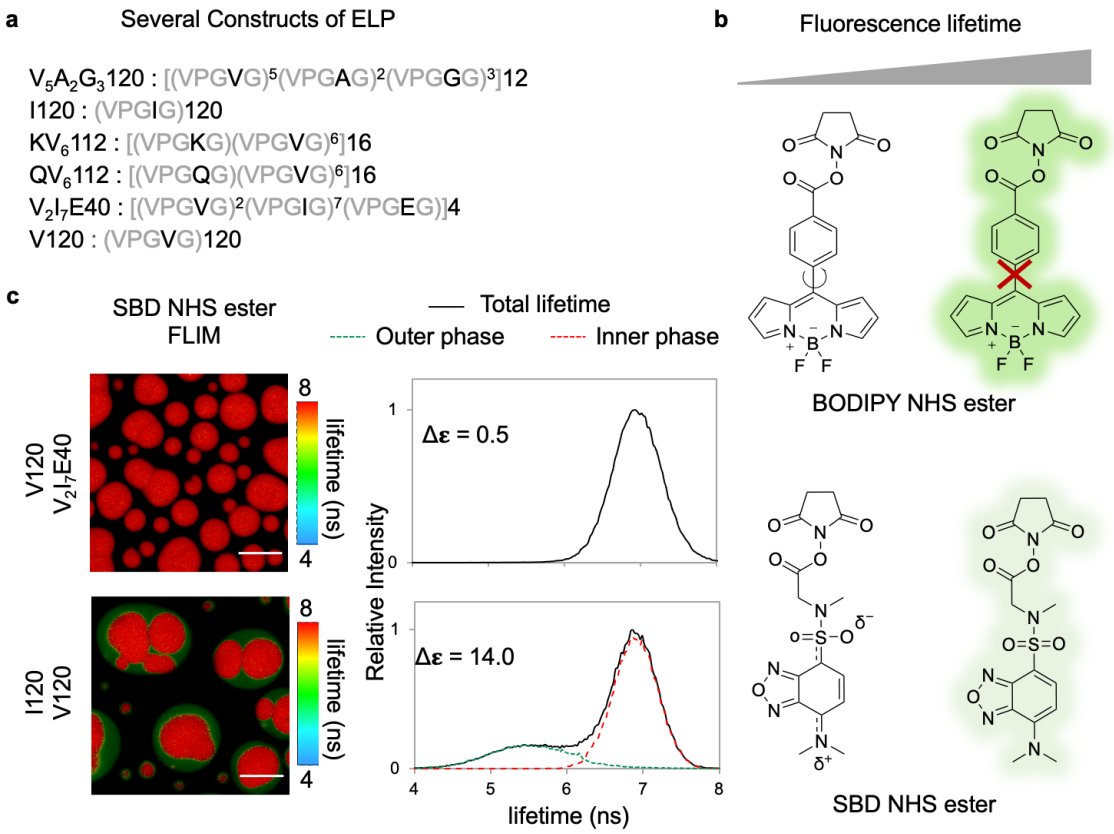

Figure **2-1**: (a) Representations of several ELPs used in the study. (b) Two environmental sensitive fluorophores developed in our lab. BODIPY-NHS ester is a molecular-rotor based viscosity sensitive fluorophore, its fluorescence lifetime increases when fixed in rigid environment. SBD-NHS ester is a polarity sensitive fluorophore, its fluorescence lifetime increases when localized in nonpolar environment. (c) Two distinctive examples showing the phase behavior of two-ELP system and their polarity difference Δ**ε**. Experimental data presented here is collected by Songtao.

To extend this work from ELP to natural protein sequences, we chose a combined system with tau187 and ELP V_2I_7E40 to expand the field of our interpretation. Tau187 is the disordered

region of the tubulin binding protein Tau, whose fibrillization is related to human neurodegeneration.

Tau187 and V_2I_7E40 Could Undergo Phase Separation *in vitro*

Most ELPs are known to exhibit LCST phase behavior in aqueous solutions. The free polymer chains of ELPs remain disordered and fully hydrated when it is below the transition temperature (T_t). Above T_t, the chains of ELP folds and assemble to form a phase-separated state mainly through hydrophobic interactions above T_t. It is well known that increase in salts causes a significant, concentration-dependent, decrease in T_t and an intriguing increase in the transition enthalpy (ΔH). Therefore, we monitored the T_t of V_2I_7E40 under varying salts and plotted out the phase diagram depicting the relationship between T_t and salt concentration. V_2I_7E40 remained in one homogenous phase when below T_t, however, it separated into one condensed phase enriched in macromolecules surrounding by a dilute phase with increased salts or temperature. Based on the phase diagram, V_2I_7E40 itself can only undergo phase separation under physiological salt condition (in this study we referred to 150 mM NaCl) above ~33˚C (Figure **2-2**). Therefore, we applied 40˚C as the phase separation temperature to perform all the imaging experiments that involves V_2I_7E40 to avoid any variations caused by temperature.

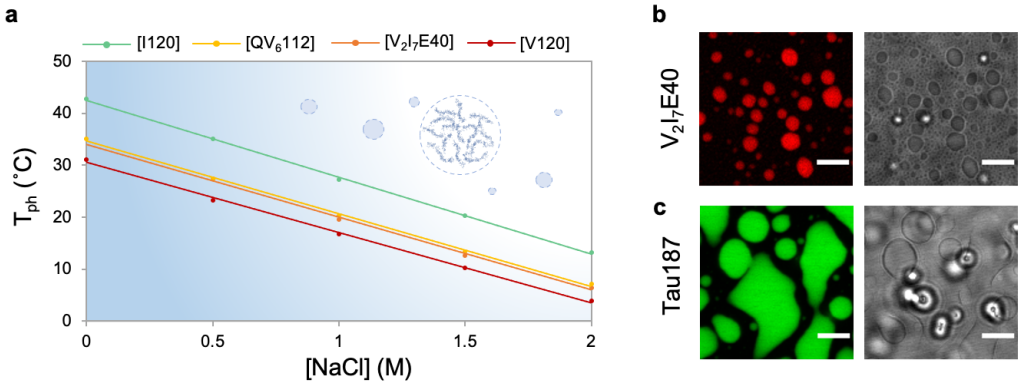

Figure **2-2**: (a) Phase transition temperature (T_t) of V_2I_7E40, I120, V120, and QV_6112 at varying salt concentration. Data collected by Songtao. Fluorescence images of (b) 70 µM V_2I_7E40 (labeled with Alexa®647) and (c) 70 µM tau187 (labeled with fluorescein) with 210 7µg/mL polyU in 20 mM HEPES, 150 mM NaCl at pH 7.0. Images collected at 40˚C. Scale bar: 10 µm.

Tau187 carries 11 positive charges at neutral pH per molecule, and for V_2I_7E40, it has 4 negative charges per molecule. Therefore, they could possibly form complex coacervates. To testify this hypothesis, we firstly monitored the phase behavior of tau187 in low salt condition and found no droplet formation at varying temperatures ranging from 0˚C up to 60˚C. Then we mixed tau187 and V_2I_7E40 together and triggered phase separation. By fluorescence microscopy we were able to observe the formation of one-layer droplets with concentrated tau187 and V_2I_7E40 evenly distributed within droplets (Figure **2-3**). In addition to V_2I_7E40, we mixed tau187 with other ELPs (V120, I120, QV_6112) and triggered phase separation of these combinations under respective temperatures (Figure **2-3**). Results indicate that tau187 mainly remains diffusive in the dilute phase surrounding ELP droplets, which suggest electrostatic interaction is the main driver in tau187 and V_2I_7E40 colocalization.

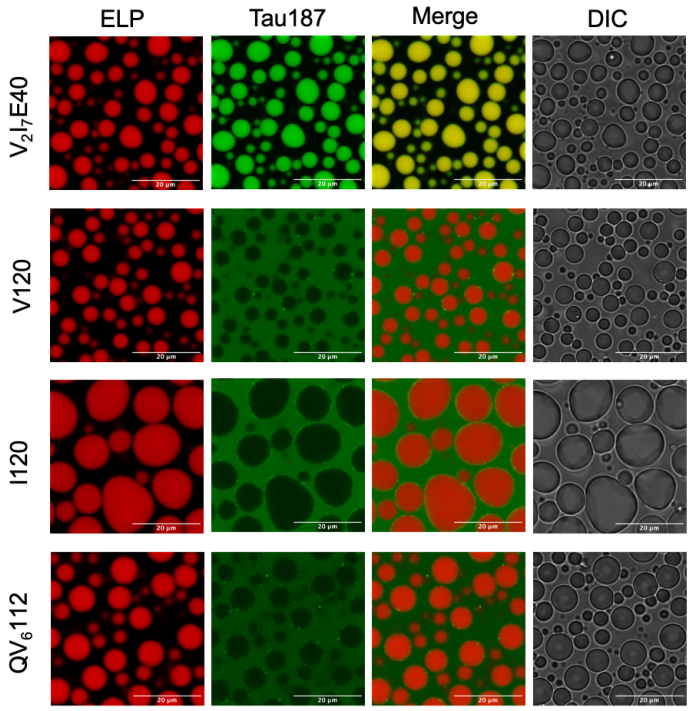

Figure **2-3**: Images of droplets formed by mixing tau187 with different ELPs. All ELPs were labeled with Alexa®647, and tau187 were labeled with fluorescein. Except for V_2I_7E40, other images were taken at 50˚C. Scale bar: 20 μm.

Modifying Bilayer Droplets by Changing the Polarity of Tau187

To measure polarity of tau187 and V_2I_7E40, we labeled tau187 and V_2I_7E40 with SBD and performed FLIM. As predicted, their lifetimes are close to each other (Figure **2-4**): 4.41 ns for tau187 ($\boldsymbol{\varepsilon}$ = 30.99) and 4.38 ns for V_2I_7E40 ($\boldsymbol{\varepsilon}$ = 31.21). The almost identical polarity explains the coacervates formed by tau187 and V_2I_7E40. To test whether increasing $\Delta\boldsymbol{\varepsilon}$ could induce layered structures, we added the third component polyU to the tau187 and V_2I_7E40 coacervates.

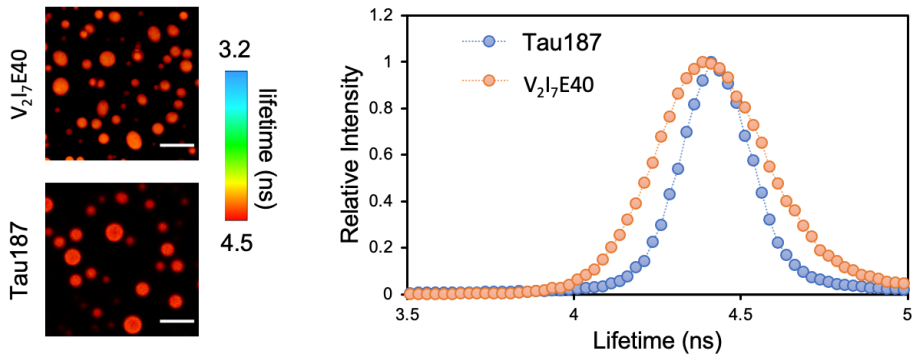

Figure **2-4**: On the left are the FLIM images of V_2I_7E40 and tau187 within coacervates in 150 mM NaCl at 40˚C. Both images were taken separately with either V_2I_7E40 labeled or tau187 labeled. On the right is the corresponding FLIM histogram. Scale bar: 10 µm.

Tau187 undergoes complex coacervation with polyU at low salt conditions *in vitro*. Thus, we mixed tau187 and polyU together at various salt conditions and observed abundant droplets formation under 500 mM NaCl and over 3 M NaCl (Figure **2-5**a, b). Given the fact that electrostatic interactions can be eliminated with excess amount of NaCl, we hypothesis that for those droplets formed over 3 M NaCl are caused by hydrophobic interactions. To validate this idea, we monitored the phase behavior of tau187 itself under different salt conditions. Remarkably, the turbidity curves of tau187 collected using UV-Vis perfectly match the previous curves of tau187-polyU over 3 M NaCl (Figure **2-5**c), which suggests that electrostatic interactions serve as the main driving force to promote tau187 phase separation in low salt conditions whereas hydrophobic interactions take over the control when in high salt conditions. To further validate the role of polyU in droplet formation, we applied RNase A to digest polyU within already formed droplets and observation was made that all the droplets disappeared within 30 min (Figure **2-5**d).

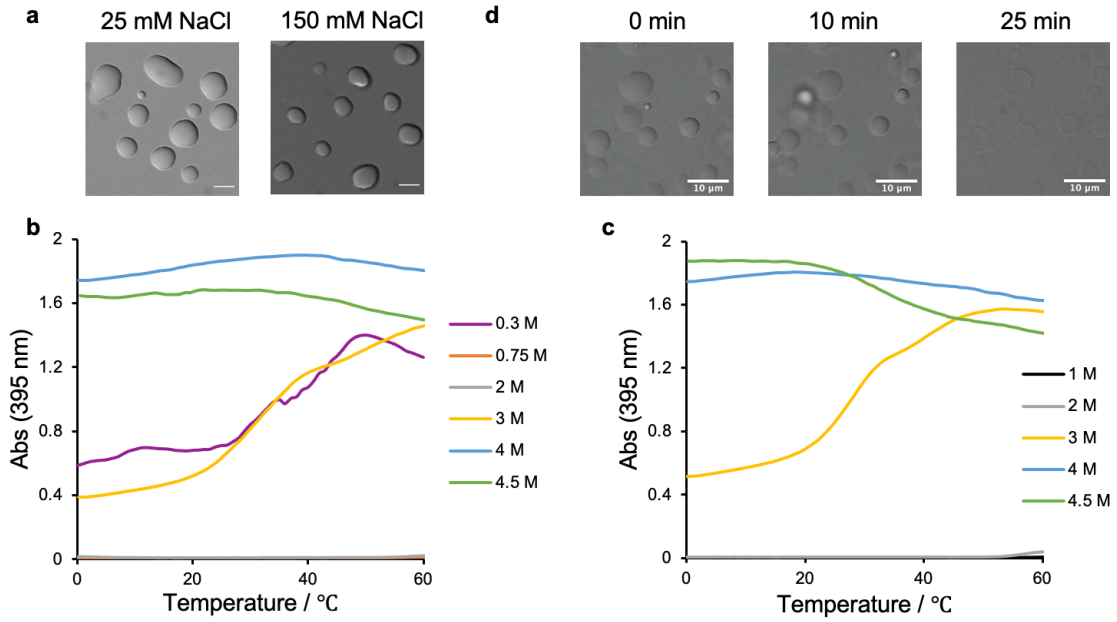

Figure **2-5**: Tau187 and polyU form complex coacervation in low salt conditions. (a) Coacervates formed by 50 μM Tau 187 and 150 μg/mL polyU. Scale bar: 5 μm. (b) and (c) UV-Vis spectrums representing the phase behaviors of (b) tau187-polyU and (c) only tau187 at different salt conditions. At NaCl concentration equal to or above 3 M, the phase behaviors of these two systems are similar, which suggested hydrophobic interactions are the main driving forces in the phase separation of tau187 at high salt conditions, regardless of polyU.

Next, we tested whether the polarity within the local environment of tau187 would change with tau187:RNA ratio. To this end, we titrated tau187 with varying amounts of polyU and tested their respective polarities using FLIM. Surprisingly, we noticed that the polarity of tau187 increases with increasing amount of polyU added (Figure **2-6**). For example, the measured polarity of tau187 is 33.36 (4.08 ns of lifetime) when only 5 μg/mL polyU is added, which continues to increase with 30 μg/mL polyU (**ε** = 34.58, 3.91 ns respectively), and 90 μg/mL polyU (**ε** = 36.58, 3.63 ns respectively). Based on this finding, we introduced polyU into tau187-V_2I_7E40 system, hoping to modify their phase behavior through the change of Δ**ε** between them.

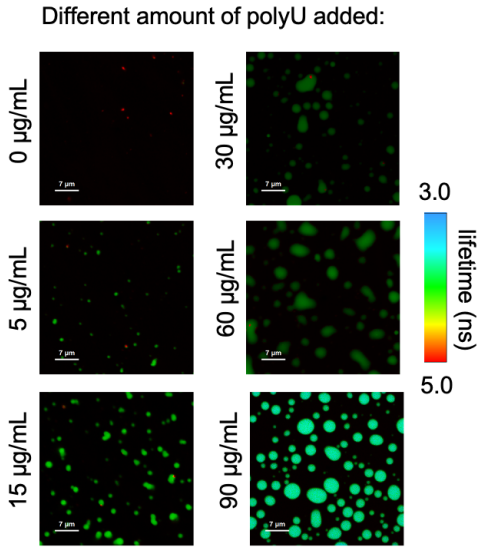

+ polyU (µg/mL)	Lifetime (ns)	Dielectric constant, ε
0	5.49	23.24
5	4.08	33.36
15	4.06	33.50
30	3.91	34.58
60	3.96	34.22
90	3.63	36.59

Figure **2-6**: FLIM images of tau187-polyU coacervates (only tau187 was labeled) with varying amount of polyU. On the right are the relative lifetime and calculated dielectric constant. We could see the polarity of tau187 increases with elevated polyU.

To ensure this strategy is feasible, we firstly monitored the phase behavior of this triple-component system through fluorescence imaging with different amount of polyU (Figure **2-7**). Through increasingly amount of polyU added, we noticed that tau187 was slowly "dragged" out of V_2I_7E40 core, emerging from fully miscible droplets (no polyU), to partially miscible droplets (5 to 90 µg/mL polyU), and eventually to two distinct droplets close to each other (equal to or more than 90 µg/mL polyU). Further quantifications of their relative fluorescence intensity ratios in the core and shell of droplets suggested an unfavored mixing between tau187 and V_2I_7E40 with increasing amount of polyU added. Interestingly, even though tau187 and V_2I_7E40 form two immiscible droplets with excessing amount of polyU added, tau187 droplets are always connected to V_2I_7E40 droplets and vice versa, which can be explained by electrostatic interactions among the edges of droplets.

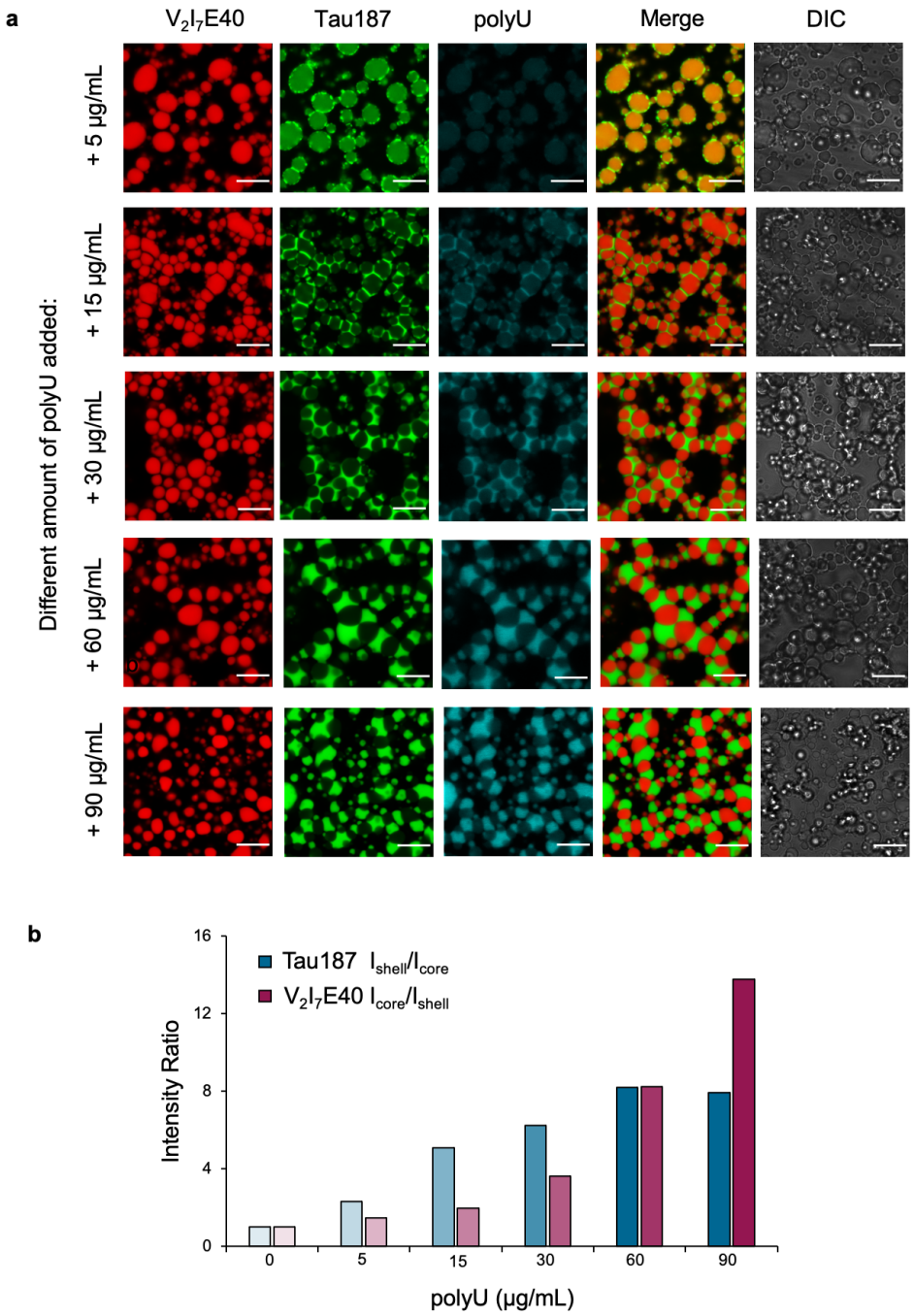

Figure **2-7**: (a) Fluorescent images of three-component system with tau187, V_2I_7E40, and varying polyU. V_2I_7E40 was labeled with coumarin, tau187 was labeled with fluorescein, and polyU was labeled with Alexa®647 respectively. (b) The partition of V_2I_7E40 and tau187 in core-shell structure was calculated by fluorescence intensity ratio, which is determined by the intensity of rich phase to the poor phase. For example, for tau187 that located in the shell, the intensity ratio is calculated

by its intensity in the shell to the intensity in the core. With increasing amount of polyU, there is decreasing co-localization of tau187 and V_2I_7E40.

After confirming that the phase behavior of tau187-V_2I_7E40 can be adjusted using polyU, we testified the polarity of each component separately (Figure **2-8**a). Firstly, by comparing the polarity of tau187 in the multicomponent system, we could see a significant increase in the polarity of tau187 from 30.99 (4.41 ns, no polyU), to 35.87 (3.73 ns, 90 μg/mL polyU). However, the polarity of V_2I_7E40 barely changed, which ranges from 30.27 (4.51 ns, 30 μg/mL polyU) to 31.21 (4.38 ns, no polyU). This suggests that polyU can still be applied to change the polarity of tau187 with the coexistence of another component V_2I_7E40. Then, we calculated the $\Delta\boldsymbol{\varepsilon}$ between tau187 and V_2I_7E40 at respective concentrations of polyU. The $\Delta\boldsymbol{\varepsilon}$ is negligible when there is no polyU added (Figure **2-8**b), and tau187 and V_2I_7E40 perfectly colocalized together. However, with the addition of polyU, $\Delta\boldsymbol{\varepsilon}$ changed from 0.22 (no polyU) to 4.66 (90 μg/mL polyU).

a

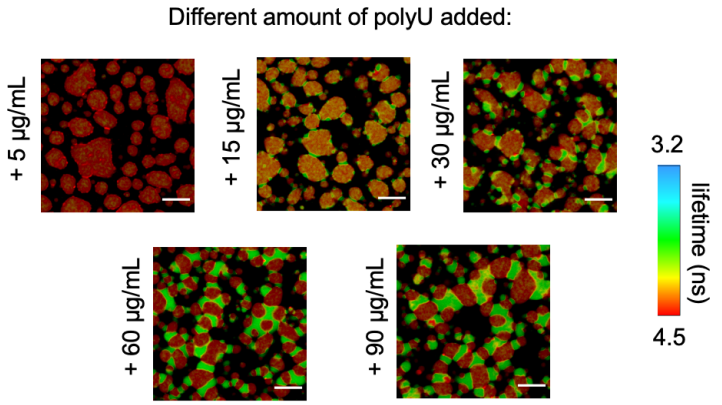

b

+ polyU (µg/mL)	Lifetime (ns)		Dielectric Constant, ε		Δε
	Tau187	V_2I_7E40	Tau187	V_2I_7E40	$\lvert\varepsilon_{tau187} - \varepsilon_{V2I7E40}\rvert$
0	4.41	4.38	30.99	31.21	0.22
5	4.31	4.44	31.71	30.78	0.93
15	4.11	4.38	33.15	31.21	1.94
30	4.21	4.51	32.43	30.27	2.16
45	4.08	4.44	33.36	30.78	2.58
60	3.93	4.41	34.44	30.99	3.45
90	3.73	4.38	35.87	31.21	4.66

Figure **2-8**: (1) FLIM images of tau187- V_2I_7E40, both proteins were labeled with SBD. (b) Relative fluorescence lifetime shown in (a), and calculated dielectric constant. The last column on the right shows the net polarity difference quantified by **Δε**.

The viscosity change in multiphase droplets formation is also characterized. Here, I labeled tau187 with viscosity sensitive fluorophore BODIPY, and monitored relative viscosity through FLIM (Figure **2-9**). It is notifying that longer fluorescence lifetime measured corresponds to higher viscosity within local environment. With the addition of polyU, tau187 exhibited two distinct

fluorescence lifetimes at the core and shell of the droplets, which suggested two disparate viscosities. The shell of the droplets showed a shorter fluorescence lifetime than the core, suggesting that the viscosity of the shell is lower.

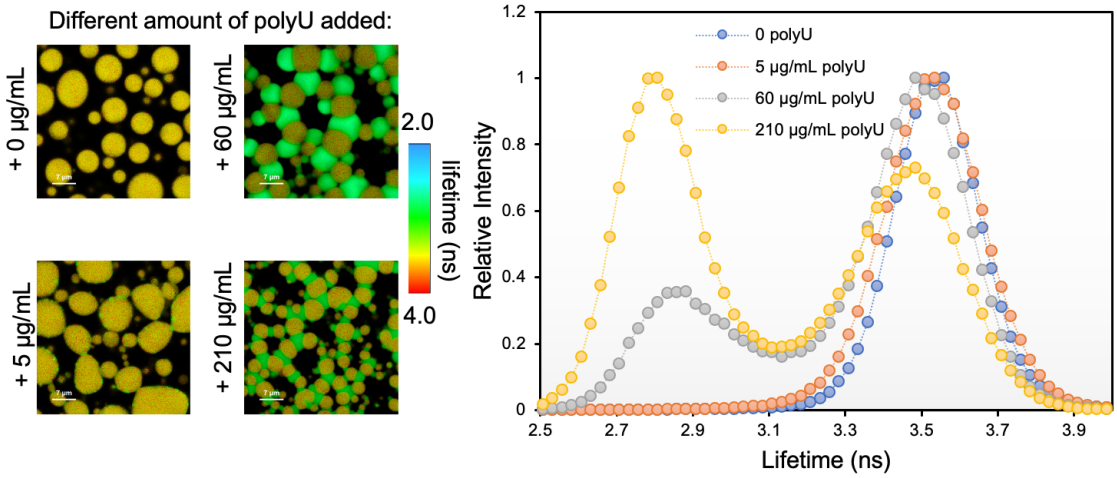

Figure **2-9**: (a) FLIM images of tau187 in three-component droplets at varying concentrations of polyU. (b) FLIM spectrum of tau187 in (a).

Chapter 3

MATERIALS AND METHODS

Plasmids

Tau187-His: Tau187-His was constructed by the Zhang laboratory from Tau 2N4R-His using the QC method. Tau 2N4R-His was purchased from Addgene and subcloned into pET9b vector.

Elastin-like polypeptides: ELPs were generous gifts from Paul Cremer laboratory and subcloned into pET29b vector.

Protein Expression and Purification

For tau187 (residues 255-441 with a His-tag fused to the C-terminus) used for *in vitro* studies, plasmids were transformed into E. coli BL21 (DE3) cells. Single colony was picked up and inoculated into 5 mL luria broth (LB) containing 100 μg/mL ampicillin, followed by serial dilution to 100 mL LB with 10^4 fold. The cultures were allowed to grow overnight at 37˚C with shaking at 220 rpm. When OD_{600} reached 0.6-0.8, 15 mL of starting culture was introduced into a culture flask containing 1.5 L freshly made LB with 100 μg/mL ampicillin. Culturing and inoculation were performed at 37˚C with shaking at 220 rpm. Inducing the expression of recombinant protein with 750 μL 1 M IPTG (a final concentration of 0.5 mM) when OD_{600} reached 0.7-0.8 and allowing it to shake overnight at 18˚C. Harvested cells by centrifugation at 5000 × g for 15 min at 4˚C and resuspended the cell pellets in buffer A (20 mM sodium phosphate, pH 7.0, 500 mM NaCl and 10 mM imidazole), stored at -80˚C until use. To carry out protein purification, cells were thawed and lysed by sonication (6 min of on time, 2 sec on, 8 sec off, 60% amplitude) on ice in the presence of

1 mM phenylmethyl sulfonyl fluoride (PMSF). The lysate was cleared out by centrifuging at 16,000 g for 60 min at 4˚C. Supernatant was collected and loaded onto a 6 mL pre-charged IMAC column (ProfinityTM IMAC Resin, Bio-Rad), followed by a washing step with 30 mL wash buffer (20 mM sodium phosphate, pH 7.0, 1 M NaCl and 10 mM imidazole) and 10 mL buffer A. Purified tau187 was then eluted with gradient addition of buffer B (20 mM sodium phosphate, pH 7.0, 500 mM NaCl and 500 mM imidazole) with varying amounts of imidazole from 10 mM to 500 mM. The elution fractions were analyzed by SDS-PAGE, and the fractions containing tau187 proteins were collected and concentrated using a centrifugal filter (MW cut off 3,000 Da) and loaded onto a gel filtration column (HiPrepTM 16/60 SephacrylTM S200HR, GE Healthcare) to get rid of DNA/RNA contamination and buffer exchange (20 mM HEPES, pH 7.0, 500 mM NaCl). The resulted protein fractions were analyzed by SDS-PAGE, and the fractions containing pure tau187 were collected and concentrated. Protein concentration were determined by absorbance at A_{274} using an extinction coefficient ε_{274} = 2.8 cm^{-1} mM^{-1}, calculated from absorption of tyrosine [4]. Flash freeze and stored at -80˚C until use. The expression and purification could be found elsewhere [3].

For ELPs used for *in vitro* studies, plasmids were transformed into E. coli BL21 (DE3) cells. Single colony was picked up and inoculated into 5 mL terrific broth (TB) containing 100 μg/mL ampicillin, followed by serial dilution to 100 mL TB with 10^4 fold. The cultures were allowed to grow overnight at 37˚C with shaking at 220 rpm. When OD_{600} reached 0.6-0.8, 15 mL of starting culture was introduced into a culture flask containing 1 L freshly made TB with 100 μg/mL ampicillin. Culturing and inoculation were performed at 37˚C with shaking at 220 rpm. Inducing the expression of recombinant protein with 1 mL 1 M IPTG (a final concentration of 1 mM) when OD_{600} reached 0.8 and allowing it to shake for 24 h at 37 ˚C. *E. coli* cultures were harvested by centrifugation at 5,000 × g for 15 min at 4˚C. Cell pellets were resuspended the in PBS buffer and stored at -80˚C until purification. For the purification of ELPs, we applied the

inverse transition cycling (ITC) that developed originally in Chilkoti lab [5], which exploits the unique phase transition behavior of ELP. The frozen cultures were thawed and one tablet of EDTA-free protease inhibitor cocktail (cOmplete™, Millipore Sigma) was added before sonication as previously described in tau187 purification. And the lysate was centrifuged at 16,000 × g for 60 min at 4˚C. Collected supernatant and added polyethyleneimine (0.5 % final concentration w/v) to precipitate DNA/RNA. Centrifuged the resulting mixture at 16,000 × g for 30 min at 4˚C. Saved the supernatant and added solid NaCl (final concentration 2 M) into the solution to precipitate ELP. Incubated the solution at 50˚C for 60 min, then centrifuged at 5,000 × g for 60 min at 40˚C. Discarded the supernatant and re-dissolved the ELP in cold PBS with gently shaking and vortexing at 4˚C overnight. Remove insoluble matter using centrifugation at 16,000 × g for 30 min at 4˚C. Then repeated the cycle of precipitating ELP by adding NaCl, followed by re-dissolve in cold PBS buffer for 2 to 3 times. The final supernatant was then dialyzed into dd H_2O at 4˚C and concentrated. Protein concentrations were determined by absorbance at A_{280} using an extinction coefficient ε_{280} = 5.69 cm^{-1} mM^{-1}. Flash freeze and stored at -80˚C until use.

Protein and RNA Labeling

Alexa® 647-NHS ester, Coumarin-NHS ester, and SBD-NHS ester were used to label the N-terminus of the ELPs through reactions with primary amines (-NH_2). The conjugation process usually takes two steps: (1) the chemical reaction, and (2) remove of excess, free NHS-ester modification. Firstly, diluted ELP in sodium bicarbonate buffer (pH 8.4) to reach final concentration around 300 mM. Dissolved respective NHS fluorophores in DMSO to make a stock solution. Then added the fluorophore solution directly into diluted ELP solution at 5 to 1 molar ratio with a total volume of 1 mL. The resulted mixture was kept in the dark at room temperature for 4h to allow enough time for labeling. Then removed the excess, free fluorophores using PD-25

column. Collected and concentrated the elution, flash freeze and stored at -80˚C until use. For all the ELPs used in fluorescence imaging and FLIM experiments, they were 5% labeled with fluorophores by mixing labeled proteins with unlabeled ones.

Fluorescein-maleimide and SBD maleimide were used to label tau187 through their reaction with cysteine residues. Diluted concentrated tau187 in 20 mM sodium phosphate buffer, 150 mM NaCl, pH 7.0. Then added EDTA into the solution at a final concentration of 5 mM to prevent metal-catalyzed formation of disulfide bonds. Dissolved respective fluorophores in DMSO to make a stock solution. Then added the fluorophore solution directly into diluted tau187 solution at 25 to 1 molar ratio with a total volume of 1 mL. The solution was then kept in the dark and allowed to proceed overnight at 4˚C. Then removed the excess, free fluorophores using PD-25 column. Collected and concentrated the elution, flash freeze and stored at -80˚C until use. For tau187 used in fluorescence imaging and FLIM experiments, it was 5% labeled with fluorophores by mixing labeled proteins with unlabeled ones.

PolyU (MW 800-1,000 kDa, Sigma #P9528) was labelled on the 3'-ends using coumarin hydrazide (Sigma #36798). PolyU was firstly dissolved in sodium acetate buffer with pH 5.2 and incubated with freshly prepared sodium periodate at room temperature for 90 min, which allows ring-opening on the 3'-terminal ribose. Then diluted the solution using sodium acetate buffer and precipitated the RNA by the addition of pure ethanol. After incubation in dry ice for 1h, centrifuged the solution at 21,000 g for 1h at 4˚C to collect precipitations. Then the pellet was resuspended in sodium acetate buffer to resolubilize polyU. Added 2 μL of 10 mM hydrazide dye into the solution and incubated the reaction in the dark at 4˚C overnight to make a conjugate with the dye. To remove all free dyes, another round of precipitation was conducted. The resulted RNA pellet was heated to get rid of ethanol and redissoled in ddH_2O. Measure the absorbance at 260 nm to calculate the concentration of RNA and at the desired excitation wavelength for the fluorophore to calculate

fraction of the RNA 3'-end-labeled with the fluorophore using NanoDrop. Then flashed freeze and stored it at -80˚C until use.

UV-Vis Spectroscopy

The turbidities of tau187 itself and tau187-polyU coacervates were measured by UV-Vis with the absorbance at 395 nm using Agilent Carey 300 UV-Vis spectrophotometer. Temperature was set to increase from 0˚C to 60˚C with a speed of 1˚C/min. 50 μM tau187 and 150 μg/mL polyU were mixed at room temperature in 20 mM HEPES buffer, pH 7.0. Then the mixture was transferred into cuvette and was allowed to incubate at 0˚C for 5 min before starting the assay.

Fluorescence Microscopy and FLIM Microscopy

For the bright field images of tau187-polyU coacervates, 50 μM tau187 and 150 μg/mL polyU were mixed at room temperature in 20 mM HEPES buffer pH 7.0 with varying salt conditions. These procedures were conducted at room temperature.

As for all the fluorescence imaging and FLIM measurements, 70 μM tau187 and 70 μM V_2I_7E40 were mixed first at room temperature, followed by the addition of certain amount of polyU. Then incubated in 40˚C for 10 min before measurements.

Dielectric Constant-Lifetime Curve Fitting

This part was carried out by Songtao Ye, another graduate student at the Zhang groug. Dissolved SBD fluorophore in different protic solvents and performed FLIM experiments to get the fluorescence lifetime of each solvent. These protic solvents already have known dielectric

constant, such as t-butanol (10.9), benzyl alcohol (11.9), 1-butanol (17.5), 2-proponol (17.9), ethanol (24.5), methanol (32.7) and ethylene glycol (37.0). Therefore, by plotting the lifetime with their known dielectric constant we could get the standard curve. (Figure **3-1**, $R^2 = 0.82$)

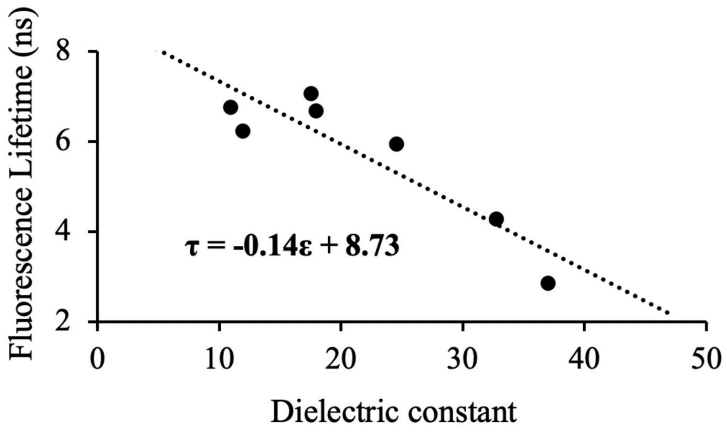

Figure **3-1**: Standard curve between polarity and fluorescence lifetime. Figure adapted from Doctorial dissertation of Songtao Ye.

Chapter 4

CONCLUSIONS

Research in past few years has made significant steps towards the understanding of biological and physiochemical mechanism that regulates the formation, organization, and biological function of membraneless organelles. Most recent findings in our lab based on artificial polypeptides suggested an indispensable role of polarity in regulating the phase separation of multicomponent systems: components with similar polarities are prone to form one condensed phase, whereas components with distinct polarities are more likely to form multilayer condensates. Moreover, the polarity of subcomponents in the outer shell are found to be higher than the polarity in the inner core. To testify whether this rule will apply to other systems, we mixed an endogenous protein tau187 and negatively charged ELP V_2I_7E40 and change the polarity of tau187 with the intention to tune their organization within droplets. With the notification that polarity of tau187 increases whereas the polarity of V_2I_7E40 remains the same with increasing amount of polyU added, we were able to "drag" tau187 from the inner core of V_2I_7E40 to the outer shell, and ultimately formed droplets with "core-shell" structure. This observation, together with previous findings on ELPs, suggests a general principle that could be utilized in the understanding of organizations in membraneless organelles and potentiates a new perspective in modifying biological condensates with desired functions.

However, questions regarding the cause of the polarity change remain elusive. Why does the polarity of tau187 droplets increase with the additional amount of polyU? Does this process correlate to general electrostatic interactions among charged residues or have something to do with specific chemical structures? Till now, all the proteins we studied are intrinsically disordered and are positively or negatively charged. However, there are plenty of proteins within membraneless

organelles have ordered structures or possess little charged residues, does the polarity rule also apply to them? Will the principle stand the ground *in-vivo* studies? Hopefully with detailed dissection of the underlying principle that regulates the polarity of macromolecule condensates, we could have better perspective on phase transition and regulation of biological condensates, and even been able to manipulate cellular process by tuning phase behaviors.

REFERENCES

1. Pederson, T. "The nucleolus." *Cold Spring Harbor Perspectives in Biology* 3.3 (2011): a000638.

2. Correll, C.C.; Bartek, J.; and Dundr, M. "The nucleolus: a multiphase condensate balancing ribosome synthesis and translational capacity in health, aging and ribosomopathies." *Cells* 8.8 (2019): 869.

3. Sawyer, I.A.; Sturgill, D.; *et al.* "Cajal body function in genome organization and transcriptome diversity." *Bioessays* 38.12 (2016): 1197-1208.

4. Brangwynne, C.P.; Eckmann, C.R.; *et al.* "Germline P granules are liquid droplets that localize by controlled dissolution/condensation." *Science* 324.5935 (2009): 1729-1732.

5. Brangwynne, C.P.; Tompa, P.; and Pappu, R.V. "Polymer physics of intracellular phase transitions." *Nature Physics* 11.11 (2015): 899-904.

6. Gomes, E.; and Shorter, J. "The molecular language of membraneless organelles." *Journal of Biological Chemistry* 294.18 (2019): 7115-7127.

7. Carter, G.C.; Hsiung, C.-H.; *et al*. "N-terminal Domain of TDP43 Enhances Liquid-Liquid Phase Separation of Globular Proteins." *Journal of Molecular Biology* 433.10 (2021): 166948.

8. Wiedner, H.J.; and Giudice, J. "It's not just a phase: function and characteristics of RNA-binding proteins in phase separation." *Nature Structural & Molecular Biology* 28.6 (2021): 465-473.

9. Uversky, V.N.; Kuznetsova, I.M.; *et al*. " Intrinsically disordered proteins as crucial constituents of cellular aqueous two phase systems and coacervates." *FEBS Letters* 589.1 (2015): 15-22.

10. Nott, T.J.; Petsalaki, E.; *et al*. "Phase transition of a disordered nuage protein generates environmentally responsive membraneless organelles." *Molecular Cell* 57.5 (2015): 936-947.

11. Cleveland, D.W.; Hwo, S.-Y.; and Kirschner, M.W. "Physical and chemical properties of purified tau factor and the role of tau in microtubule assembly." *Journal of Molecular Biology* 116.2 (1977): 227-247.

12. Jouanne, M.; Rault, S.; and Voisin-Chiret, A.-S. "Tau protein aggregation in Alzheimer's disease: an attractive target for the development of novel therapeutic agents." *European Journal of Medicinal Chemistry* 139 (2017): 153-167.

13. Falcon, B.; Zhang, W.; *et al.* "Structures of filaments from Pick's disease reveal a novel tau protein fold." *Nature* 561.7721 (2018): 137-140.

14. Ingram, E.M.; and Spillantini, M.G. "Tau gene mutations: dissecting the pathogenesis of FTDP-17." *Trends in Molecular Medicine* 8.12 (2002): 555-562.

15. Zhang, W.; Tarutani, A.; *et al*. "Novel tau filament fold in corticobasal degeneration." *Nature* 580.7802 (2020): 283-287.

16. Vanderweyde, T.; Apicco, D.J.; *et al*. "Interaction of tau with the RNA-binding protein TIA1 regulates tau pathophysiology and toxicity." *Cell Reports* 15.7 (2016): 1455-1466.

17. Kar, S.; Fan, J.; *et al.* "Repeat motifs of tau bind to the insides of microtubules in the absence of taxol." *The EMBO Journal* 22.1 (2003): 70-77.

18. Guo, T.; Noble, W.; and Hanger, D.P. "Roles of tau protein in health and disease." *Acta Neuropathologica* 133.5 (2017): 665-704.

19. Derisbourg, M.; Leghay, C.; *et al.* "Role of the Tau N-terminal region in microtubule stabilization revealed by newendogenous truncated forms." *Scientific Reports* 5.1 (2015): 1-10.

20. Zhang, X.; Lin, Y.; *et al.* "RNA stores tau reversibly in complex coacervates." *PLOS Biology* 15.7 (2017): e2002183.

21. Lin, Y.; McCarty, J.; *et al*. "Narrow equilibrium window for complex coacervation of tau and RNA under cellular conditions." *eLife* 8 (2019): e42571.

22. Jho, Y.; Yoo, H.Y.; *et al*. "Molecular and structural basis of low interfacial energy of complex coacervates in water." *Advances in Colloid and Interface Science* 239 (2017): 61-73.

23. Dai, M.; Georgilis, E.; *et al*. "Refining the Design of Diblock Elastin-Like Polypeptides for Self-Assembly into Nanoparticles." *Polymers* 13.9 (2021): 1470.

24. Urry, D.W. "Physical chemistry of biological free energy transduction as demonstrated by elastic protein-based polymers." *The Journal of Physical Chemistry B* 101.51 (1997): 11007-11028.

25. Wise, S.G.; and Weiss, A.S. "Tropoelastin." *The International Journal of Biochemistry &Cell Biology* 41.3 (2009): 494-497.

26. Roberts, S.; Dzuricky, M.; and Chilkoti, A. "Elastin-like polypeptides as models of intrinsically disordered proteins." *FEBS Letters* 589.19 (2015): 2477-2486.

27. Zhao, C.; Ma, Z.; and Zhu, X.X. "Rational design of thermoresponsive polymers in aqueous solutions: A thermodynamics map." *Progress in Polymer Science* 90 (2019): 269-291.

28. Zhang, Q.; Weber, C.; *et al*. "Thermoresponsive polymers with lower critical solution temperature: from fundamental aspects and measuring techniques to recommended turbidimetry conditions." *Materials Horizons* 4.2 (2017): 109-116.

29. Rosa, V.R.; Woisel, P.; and Hoogenboom, R. "Supramolecular control over thermoresponsive polymers." *Materials Today* 19.1 (2016): 44-55.

30. Varanko, A.K.; Su, J.C.; and Chilkoti, A. "Elastin-like polypeptides for biomedical applications." *Annual Review of Biomedical Engineering* 22 (2020): 343-369.

31. Feric, M.; Vaidya, N.; *et al*. "Coexisting liquid phases underlie nucleolar subcompartments." *Cell* 165.7 (2016): 1686-1697.

32. Boisvert, F.-M.; Koningsbruggen, S.; *et al*. "The multifunctional nucleolus." *Nature Reviews Molecular Cell Biology* 8.7 (2007): 574-585.

33. Simon, J.R.; Carroll, N.J.; *et al*. "Programming molecular self-assembly of intrinsically disordered proteins containing sequences of low complexity." *Nature Chemistry* 9.6 (2017): 509-515.

34. Lu, T.; and Spruijt, E. "Multiphase complex coacervate droplets." *Journal of the American Chemical Society* 142.6 (2020): 2905-2914.

35. Liu, Y.; Miao, K.; *et al*. "A HaloTag-based multicolor fluorogenic sensor visualizes and quantifies proteome stress in live cells using solvatochromic and molecular rotor-based fluorophores." *Biochemistry* 57.31 (2018): 4663-4674.

36. Hoelzel, C.A.; and Zhang, X. "Visualizing and Manipulating Biological Processes Using HaloTag and SNAP-Tag Technologies." *Chembiochem: a European Journal of Chemical Biology* 21.14 (2020): 1935.

37. Teo, W.; Carprariello, A.V.; *et al.* "Nile Red fluorescence spectroscopy reports early physicochemical changes in myelin with high sensitivity." *Proceedings of the National Academy of Sciences* 118.8 (2021).

38. Pazin, W.M.; Almeida, A.K.A.; *et al*. "Thermal and solvatochromic effects on the emission properties of a thienyl-based dansyl derivative." *Royal Society of Chemistry Advances* 10.48 (2020): 28484-28491.

39. Dziuba, D.; Pospíšil, P.; *et al*. "Solvatochromic fluorene-linked nucleoside and DNA as color-changing fluorescent probes for sensing interactions." *Chemical Science* 7.9 (2016): 5775-5785.

40. Zhuang, Y.-D.; Chiang, P.-Y.; *et al.* "Environment-sensitive fluorescent turn-on probes targeting hydrophobic ligand-binding domains for selective protein detection." *Angewandte Chemie* 125.31 (2013): 8282-8286.

41. Datta, R.; Heaster, T.M.; *et al.* "Fluorescence lifetime imaging microscopy: fundamentals and advances in instrumentation, analysis, and applications." *Journal of Biomedical Optics* 25.7 (2020): 071203.